Structure, Dynamics, and Electronic Properties of Cobaltocene in $SnS_{2-x}Se_x\{0 \leqslant x \leqslant 2\}$

D. O'Hare
Inorganic Chemistry Laboratory, South Parks Road, Oxford OX1 3QR

1 Introduction

Two-dimensional layered materials, such as the tin dichalcogenides $SnS_{2-x}Se_x$ ($0 \leqslant x \leqslant 2$), have been much studied with regard to their pronounced electronic and structural anisotropy.[1] The $SnS_{2-x}Se_x$ layered compounds crystallize in the $Cd(OH)_2$-type structure (space group $P\bar{3}m1$) to form an isostructural series of solid solutions.[2] The three-dimensional structure is built from repeatedly stacked XMX lamellae bound together by van der Waals interactions between adjacent planes of hexagonally close-packed chalcogenide atoms (X). In SnX_2 (X = S, Se) the metal atoms are coordinated in nearly octahedral sites (Figure 1).

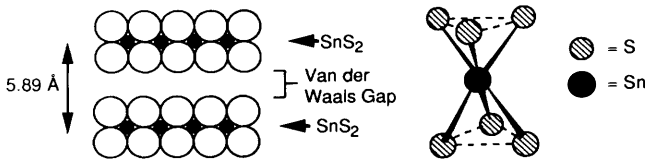

Figure 1 Representation of the octahedral $Cd(OH)_2$ type structure of SnS_2.

The layered MX_2 structure permits a variety of guest molecules to be inserted into the interlamellar gaps of the host materials.[3] For example, the intercalation of metallic tantalum and niobium dichalcogenides by organic amines has led to the discovery of a new class of two-dimensional superconductors.[4] This has raised questions as to the dimensionality of superconductivity in layered structures and the relationship between charge density waves (CDWs) and the superconducting BCS mechanisms.[5]

There are also many examples of semiconducting layered structures being induced into a metallic state by intercalation of electron-donor guest species, for example, $LiTiS_2$,[6] $K_{0.5}WS_2$,[7] and $K_{0.5}MoS_2$.[8] The importance of electron-transfer from the guest to the host in these intercalation reactions has been recognized for some time.[9] In view of this, the possibility of fine-tuning the electronic structure of the host material by intercalation has led to a vast effort towards the synthesis and characterization of layered MX_2 materials (M = Ti, Mo, W, Ta, Nb; X = S, Se) intercalated by molecular guests such as hydrazine, organic amines, and metallocenes.[10] Almost no interest has been shown towards the intercalation of non-transition metal dichalcogenides such as SnS_2 and $SnSe_2$.[11]

This paper reviews our research over the past 18 months on the detailed characterization of the organometallic intercalates $SnS_{2-x}Se_x\{Co(\eta\text{-}Cp)_2\}_{0.33}$ ($Cp = C_5H_5$; $0 \leqslant x \leqslant 2$). Full accounts of the crystal structure,[12] photoelectron spectroscopy,[13] electronic conductivity,[14] and solid state NMR experiments[15] of these materials have been published previously.

2 Synthesis of the Intercalates $SnS_{2-x}Se_x\{Co(\eta\text{-}Cp)_2\}_{0.33\pm0.02}$

Single crystals of the $SnS_{2-x}Se_x$ hosts were all grown using the iodine vapour transport method. The high purity elements (> 99.99%) with a 1% molar quantity of phosphorus dopant and the transport agent I_2 (5 mg cm^{-3}) were sealed in evacuated quartz ampoules (10 cm × 1.7 cm). A three-zone furnace provided a stable temperature gradient between the reaction zone (685 °C for SnS_2) and the growth zone (645 °C for SnS_2).

The intercalates were prepared by adding the crystalline host (*ca.* 100 mg) to a solution of freshly sublimed $Co(\eta\text{-}Cp)_2$ (*ca.* 150 mg) in acetonitrile (*ca.* 5 cm^3) under a nitrogen atmosphere. In order to avoid damage to the brittle crystals the reaction was carried out at *ca.* 65 °C without stirring. After the reaction was complete, typically 5—21 days, the $Co(\eta\text{-}Cp)_2$ solution was removed and the intercalate washed with acetonitrile (4 × 20 cm^3) until the filtrate was colourless. The product crystals were deemed to be fully intercalated when all the host reflections had disappeared from the *X*-ray powder spectrum; we observed no evidence for staging at any point during the course of these reactions. Table 1 shows the lattice expansion, stoichiometries, appearance, and reaction conditions for the intercalates produced in this study. The stoichiometry in each case was determined by elemental microanalysis.

3 Characterization of the Intercalates $SnS_{2-x}Se_x\{Co(\eta\text{-}Cp)_2\}_{0.33\pm0.02}$

3.1 *X*-Ray Crystal Structure Determination of $SnS_2\{Co(\eta\text{-}Cp)_2\}_{0.33}$

The intercalation of an organometallic species into a layered host lattice has been known since Dines reported the intercalation of cobaltocene $\{Co(\eta\text{-}Cp)_2\}$ into ZrS_2 in 1975.[16] Since then a large number of related metallocenes have been intercalated

Dermot O'Hare was educated at Balliol College, Oxford (B.A. 1982, D.Phil 1985). His D.Phil research was carried out with Professor M. L. H. Green F. R. S. on the activation of carbon–hydrogen bonds using metal atoms. In 1985 he was elected to an Exhibition of 1851 Research Fellowship and a Junior Research Fellowship at Wolfson College, Oxford. He was a temporary University Lecturer and Supernumerary Fellow of St John's College (1987—89), until his current appointment as University Lecturer in Inorganic Chemistry and Tutorial Fellow at Balliol College. He has co-authored over 60 publications and his research interests include synthetic organometallic chemistry and its applications in solid state chemistry.

Table 1 Stoichiometries, reaction conditions, lattice expansion, and appearance for some intercalated layered materials $SnS_{2-x}Se_x\{Co(\eta\text{-}Cp)_2\}_{0.33\pm0.02}\{0 \leqslant x \leqslant 2\}$

Host stoichiometry	Reaction conditions T (°C); t (days)	Guest stoichiometry	Δc (Å)	Colour
SnS_2	65;5	0.31	5.29	dark blue
$SnS_{1.7}Se_{0.3}$	65;7	0.31	5.24	light blue
$SnS_{1.5}Se_{0.5}$	65;9	0.31	5.20	light blue
$SnS_{0.7}Se_{1.3}$	65;14	0.33	5.26	black
$SnS_{0.15}Se_{1.85}$	65;17	0.33	5.50	black
$SnSe_2$	65;21	0.33	5.56	black

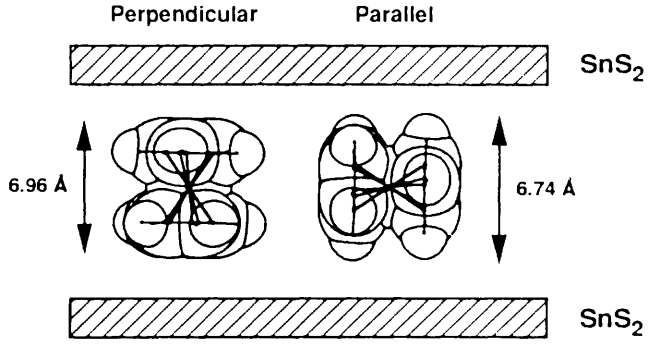

Figure 2 Van der Waals dimensions of $Co(\eta\text{-}Cp)_2$.

into layer lattices.[17] While the physical properties of these early metallocene intercalates have been extensively studied, very little is known about their structure, and fundamental questions such as the orientation of the metallocene guests within the host remain uncertain or controversial.

For example, although upon intercalation of cobaltocene into a lamellar metal dichalcogenide host the interlayer spacing typically increases from 5.89 to 11.18 Å ($\Delta c = 5.29$ Å) as measured by powder *X*-ray diffraction, due to the almost spherical shape of the cobaltocene molecule (Figure 2) little information can be determined from these lattice expansion measurements alone. However, we have recently been able to determine the three-dimensional structure of a single crystal of SnS_2 intercalated with cobaltocene. Owing to the disorder and low crystallinity of these compounds it was necessary to use conventional *X*-ray film methods of recording the diffraction pattern, and to perform the data analysis sequentially. A one-dimensional analysis of only the 00*l* reflections gave the first indication that the cobaltocene guests molecules adopt an orientation with the molecular C_5 symmetry axis parallel to the planes of the host lattice layers. Least squares refinement of the observed structure factors derived from the zero-layer Weissenberg photograph (0*kl* zone) confirmed that the cobaltocenes adopt a parallel orientation, and that the SnS_2 layers, while remaining intact on intercalation, undergo a shift relative to each other, leading to a doubling of the unit cell dimension along the *c*-axis. Finally, including all the observed reflections we derived a three-dimensional structure showing that the lattice layers shift in both the *a* and *b* directions. We believe this was the first report of a three-dimensional structure determination of an organometallic intercalate.

3.2 Neutron Diffraction Experiments on $SnS_2\{Co(\eta\text{-}C_5D_5)_2\}_{0.33}$

Comparison of the scattering factors for the constituent atoms using either *X*-rays or neutrons revealed that $Co(\eta\text{-}Cp)_2$ would contribute only 19% in an *X*-ray diffraction experiment whereas 44% of the scattering would be due to the $Co(\eta\text{-}C_5D_5)_2$ in a analogous neutron diffraction experiment. Therefore neutron diffraction should be a more sensitive probe of the metallocene orientation. A major drawback of neutron diffraction studies on organic or organometallic compounds is the large incoherent scattering of hydrogen that leads to low quality diffraction patterns. This problem is overcome by using samples with a high level of deuterium enrichment, as incoherent scattering is much lower for deuterium.

Thus time-of-flight neutron diffraction data were collected on an aligned ensemble of single crystals of $SnS_2\{Co(\eta\text{-}C_5D_5)_2\}_{0.31}$. Least squares refinement of the occupancies of an initial model containing both the parallel and perpendicular extreme orientations refined to a parallel occupancy of 0.302(5) and a perpendicular occupancy of 0.008(5). The overall agreement factor of 10.5% was achieved using a model containing a single parallel orientation for the $Co(\eta\text{-}C_5D_5)_2$ which is in excellent agreement with the *X*-ray structure refinement.

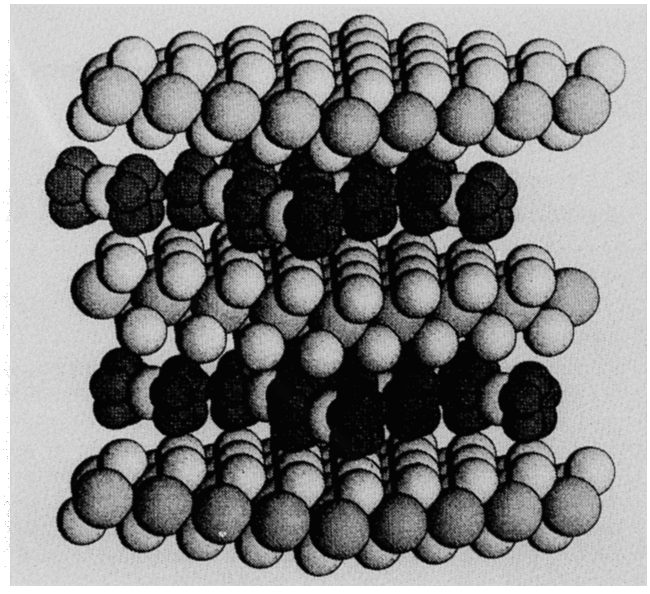

Figure 3 Van der Waals representation of the *X*-ray structure of $SnS_2\{Co(\eta\text{-}Cp)_2\}_{0.31}$.

3.3 Solid State ^2H NMR Experiments on $SnS_2\{Co(\eta\text{-}C_5D_5)_2\}_{0.31}$

In a solid state ^2H NMR experiment the energetically most significant perturbation to the nuclear energy levels is the interaction of the nuclear quadrupole of the ^2H ($I = 1$) nucleus with the external magnetic field. In the case of a deuteron in an axially symmetric environment a doublet is observed in the solid state spectrum whose separation depends on the orientation of the C–D bond with respect to the magnetic field. Thus solid state ^2H NMR is ideally suited to the study of molecular orientation and dynamics in solids.

The ^2H NMR spectra of a single crystal of $SnS_2\{Co(\eta\text{-}C_5D_5)_2\}_{0.33}$ oriented with basal plane (crystallographic *a*–*b* plane) perpendicular and parallel to the static magnetic field are shown in Figure 4. The ^2H NMR spectra are easily interpreted and immediately suggest the orientation of the cobaltocene molecules, without having to consider additional static disorder within the layers, or in-plane rotations of the cobaltocenes. In contrast to the powder lineshapes observed from a polycrystalline sample, for an orientated single crystal we should observe only one sharp doublet per orientation. If the cobaltocene molecule adopts the perpendicular orientation, then only the *x* component of the electric field gradient (e.f.g.) tensor at the deuteron, eq_{xx}, has a non-zero projection along the field direction; rotation about the $Co-Cp_{(centroid)}$ axis will have no effect on eq_{xx}. The spectrum obtained will therefore consist of a doublet with a splitting of *ca.* 136 kHz. There are two possible low-energy motional processes postulated for the parallel orientation. Rotation about the $Co-Cp_{(centroid)}$ axis will cause an averaging of the *z* and *y* components of the e.f.g., eq_{yy} and eq_{zz}, and the resulting spectrum will reflect this averaging, giving a splitting of approximately 68kHz, as shown schematically in Figure 5. Additional in-plane (*ab* plane) rotation will cause no further averaging of the e.f.g. tensor. Only one doublet is observed with a splitting of 68 kHz when the crystal is orientated perpendicular to the magnetic field, this strongly suggests that the guest molecules adopt a single orientation in the host structure: the parallel orientation.

3.4 Electrical Conductivity Experiments

The temperature-dependence of the four-probe conductivity for single crystals of both the hosts and intercalates have been measured in the temperature range 2—300 K. Figure 6a presents a plot of $\log_{10}$ Resistivity *vs.* Temperature for the entire series of

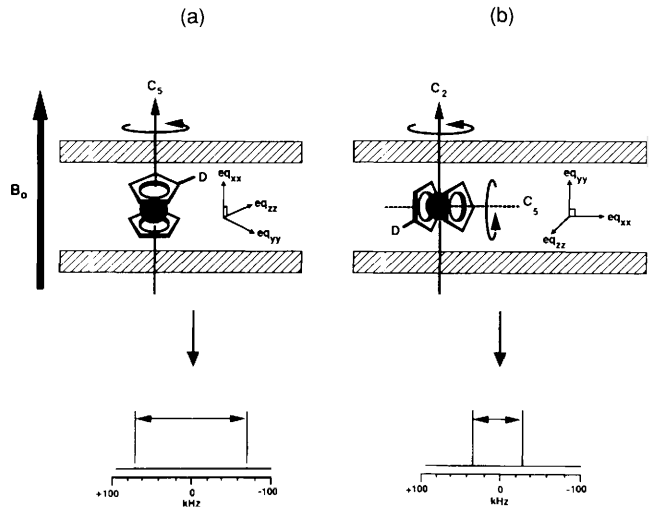

Figure 4 The postulated motions for $Co(\eta\text{-}C_5D_5)_2$ in the $^2H\text{–}SnS_2$ lattice in the perpendicular (a) and parallel (b) orientations and its predicted ^2H NMR spectra when the static magnetic field is aligned perpendicular and parallel to the basal plane.

host single crystals (phosphorus doped) $SnS_{2-x}Se_x$, where $x = 0.0, 0.3, 0.7, 1.3, 1.85$, and 2.0. This plot dramatically shows the wide variation in conductivity behaviour in the host structures as sulfur is replaced by selenium. A closer examination of the data presented in Figure 6 suggests that the host materials can be divided into two distinct classes on the basis of their resistivity variation with temperature. For class I ($x = 0.0$, 0.3, 0.7, and 1.3) the resistivity spans several orders of magnitude in the temperature range 100—300 K. For class II ($x = 1.85$ and 2.0) the resistivity decreases in the range 298 K to *ca.* 150 K then increases down to 2 K. The lowest resistivity corresponds to 140 and 160 K for $x = 1.85$ and $x = 2.0$ respectively.

Materials in class I seem to be well described by an Arrhenius-type model for conductivity. Plots of $\log_{10}$ Resistivity *vs.* T^{-1} for $SnS_{2-x}Se_x$, $\{x = 0.0, 0.3, 0.7,$ and $1.31\}$ are linear; the observed activation energies (E_a) decrease steadily from 0.45 eV ($x = 0.0$) to 0.09 eV ($x = 1.3$) across this series.

The materials in class II can be modelled by considering them to be very low activation energy semiconductors (E_a *ca.* 10^{-2} eV), so that the carrier mobility term (μ) becomes important compared to the carrier concentration (n) at elevated temperatures ($T > 150$ K). This would account for their metallic-like behaviour in the range 150—300 K. Previously, a similar temperature-dependence of the resistivity (ρ) for the organic

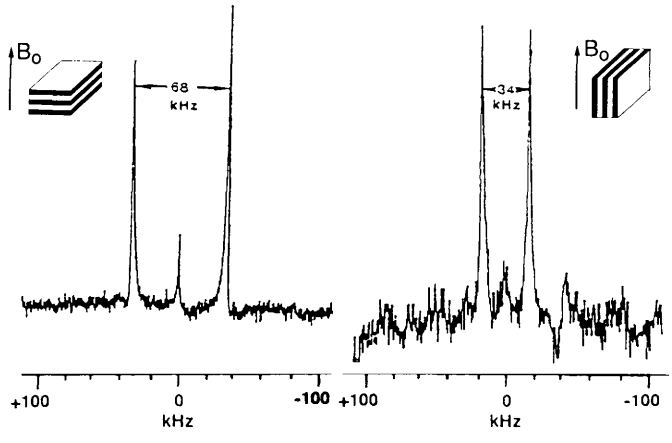

Figure 5 ^2H NMR room temperature spectra of a single crystal of $SnS_2\{Co(\eta\text{-}C_5D_5)_2\}_{0.31}$ oriented with the single crystal basal plane (a) perpendicular and (b) parallel to the static magnetic field. (The spike at 0 ppm is an artefact.)

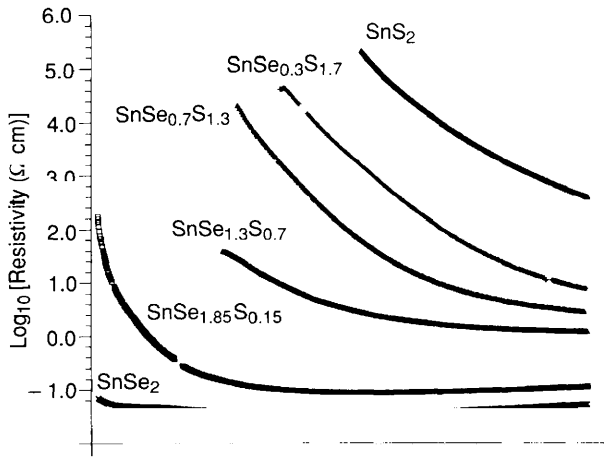

Figure 6a Plot of $\log_{10}$ Resistivity *vs.* Temperature for the host single

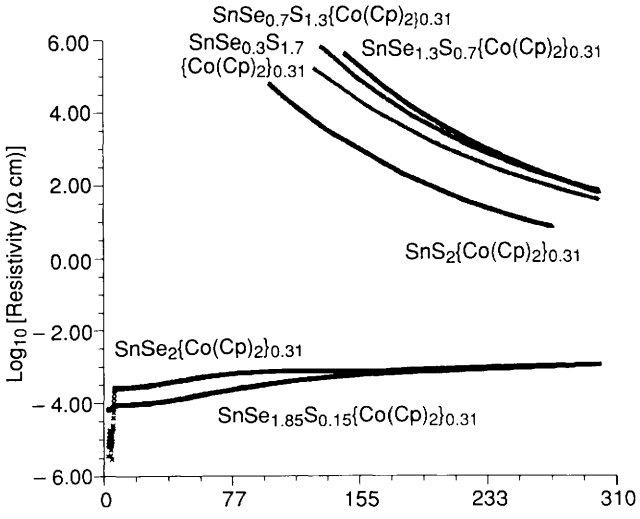

crystals, $SnS_{2-x}Se_x\{Co(\eta\text{-}Cp)_2\}_{0.33\pm0.02}$ $\{0 \leqslant x \leqslant 2\}$.

conductor $(NMP)_2TCNQ$, {NMP = *N*-methylphenazinium; TCNQ = 7,7′,8,8′-tetracyano-*p*-quinodimethane} has been modelled using equation 1.[18]

$$\rho(T) = \left(\frac{1}{ne\mu}\right) = AT^{\alpha}\exp\left(\frac{E_a}{kT}\right) \qquad (1)$$

The temperature dependence of conductivity is considered to depend on the activation energy (E_a) and the type of scattering mechanism in operation. Best fits for the resistivity *versus* temperature (100—300 K) data for $x = 1.85$ and $x = 2.0$ to the theoretical expression in equation 1 are given in Table 2. Table 2 summarizes the resistivity (ρ) at 298 K, the mobility parameter (α) and activation energy (E_a) for the host crystals $SnS_{2-x}Se_x$, $\{x = 0.0, 0.3, 0.7, 1.3, 1.85,$ and $2.0\}$.

The experimental data show a gradually decreasing activation energy in these host materials from SnS_2 (0.45 eV) to $SnSe_2$ (0.02 eV) *via* $SnS_{0.7}Se_{1.3}$ (0.09 eV). This is to be expected on the basis of Mott's impurity model for doped semiconductors,[19] which predicts that as the medium becomes more polarizable the energy required to ionize impurity electrons from the donor levels into the host conduction band will decrease. No work has been done to estimate the level of P doping throughout the series,

Table 2 Summary of important resistivity data for the hosts $SnS_{2-x}Se_x$;$\{0 \leqslant x \leqslant 2\}$

Hosts (x)	ρ (Ω cm, 298 K)	E_a (eV)	α
0.0	387.6	0.45	—
0.3	7.67	0.37	—
0.7	2.87	0.28	—
1.3	1.21	0.09	—
1.85	0.114	0.025	1.70
2.0	0.054	0.020	1.72

Table 3 Summary of important resistivity data for the intercalates $SnS_{2-x}Se_x\{Co(\eta\text{-Cp})_2\}_{0.33\pm0.02}$

Intercalates (x)	ρ (Ωcm, 298 K)	ρ_0 ($\times 10^{-10}$)	T_0 ($\times 10^8$ K)	$1/_\omega$	T_c(K)
0.0	3.90	1.54	3.67	4.0	—
0.3	38.6	7.48	3.42	3.9	—
0.7	69.2	9.77	3.60	3.9	—
1.3	61.7	12.5	3.64	3.9	—
1.85	1.1×10^{-2}	—	—	—	5.7
2.0	1.1×10^{-2}	—	—	—	6.1

but an estimate of 10^{15} cm^{-3} for the carrier density in P-doped SnS_2 has been made.[20]

The conductivity behaviour of the so-called class II host materials can be interpreted in terms of the carrier mobility factor (μ) in semiconductors with small activation energies (E_a *ca.* 10^{-2} eV). The model presented on the basis of equation 1 seems to work well above 100 K, but below this temperature there is some deviation – possibly arising from additional conduction *via* impurity sites.

It has previously been demonstrated that in two-dimensional layered systems the carrier mobility (μ) is highly temperature-dependent as in equation 2.[21]

$$\frac{\mu(T_1)}{\mu(T_2)} = \left(\frac{T_1}{T_2}\right)^{-\alpha}; \alpha > 1.5 \qquad (2)$$

This strong temperature-dependence above *ca.* 100 K has been related to an optical phonon scattering mechanism. This is unique to two-dimensional layered materials, since the carriers are confined to individual XMX layers with mainly short-range interactions coupling the carriers to the optical modes of the lattice. These vibrational modes involve modulation of the XMX sandwich thickness in layered materials.

In this study the exponent (α) in the mobility temperature-dependence expression in $SnS_{2-x}Se_x$ crystals was found to be $\alpha = 1.70$, 1.72 for $x = 1.85$, 2.0 respectively. This correlates well with theoretical predictions and other experimental data on layered systems,[21] suggesting that scattering of conduction electrons at $T > 75$ K may well be related to this mechanism in these particular $SnS_{2-x}Se_x$ hosts.

In order to illustrate clearly the difference in electrical properties of the intercalates at either end of the series, Figure 6b shows a plot of $\log_{10}$ resistivity *vs.* temperature variation for the entire intercalate single crystal series. As with the host materials it is convenient to divide the intercalate compounds into two distinct groups. Consider first the mainly sulfur-rich intercalate single crystals $SnS_{2-x}Se_x\{Co(\eta\text{-Cp})_2\}_{0.31}$, $\{x = 0.0, 0.3, 0.7,$ and $1.3\}$. For these samples a plot of $\log_{10}$ resistivity *vs.* $T^{-1/4}$ is linear, and is in excellent agreement with the Mott variable-range hopping (VRH) law. Least squares fitting of the resistivity data to equation 3[22] gives $\omega = 0.25 \pm 0.02$:

$$\rho(T) = \rho_0\left(\frac{T}{T_0}\right)^{\frac{1}{2}}\exp\left\{\left(\frac{T_0}{T}\right)^{\omega}\right\} \qquad (3)$$

The values of ρ at 298 K, ω, ρ_0, and T_0 for each composition are given in Table 3. Notice that the room temperature resistivity increases for $x = 0.3$, 0.7, and 1.3 upon intercalation, whereas for $x = 0.0$ the opposite is true. Experiments have demonstrated that there is considerable anisotropy in the host single-crystal conductivity ($\rho_\parallel/\rho_\perp$ *ca.* 100), whereas in the intercalate materials a much reduced anisotropy is observed ($\rho_\parallel/\rho_\perp$ *ca.* 10).

However, a hopping mechanism in d-dimensions yields a $T^{-(1/(1+d))}$ expression,[23] so the conductivity data for the intercalates strongly suggest an isotropic three-dimensional ($T^{-1/4}$) hopping process rather than a two-dimensional ($T^{-1/3}$) process. The experiments carried out to investigate the anisotropy of conduction in these intercalate systems suggest that the current carriers are not confined to a single layer to such an extent as in the host systems. The higher resistivity of some of these intercalates relative to their host compounds (Table 3), despite substantial electron transfer to the Sn atoms, may depend on the limiting nature of the thermally activated hopping process rather than the presence of a large energy gap.

The resistivity for the $SnS_{2-x}Se_x\{Co(\eta\text{-Cp})_2\}_{0.33\pm0.02}$ ($x = 1.85$ and 2.0) decreases with decreasing temperature as expected for metallic samples. Thus a clear semiconductor-to-metal transition appears to occur in the stoichiometry range $1.3 < x < 1.85$. Remarkably, at 5.7 K ($x = 1.85$) the resistivity drops sharply (width 1.5 K). At 6.1 K($x = 2.0$) a similar transition (width 0.7 K) is observed with the resistivity falling to zero.

This superconducting transition has been confirmed in the diselenide case by magnetic susceptibility measurements, which have demonstrated the Meissner effect below 6 K appropriate to a type II superconductor. At 4.2 K the critical fields H_{c1} and H_{c2} were 40 G and 700 G respectively. Below 3K extensive hysteresis of the magnetization is observed due to flux trapping within the samples.

In the tin dichalcogenide intercalates the superconducting transition temperature (T_c) increases as sulfur is replaced by selenium. This change can be understood in terms of the enhanced degree of electron charge transfer to the empty Sn(5*s*, 5*p*) conduction band as suggested by XPES data (*vide infra*). This can be related to the increasing polarizability of the medium as selenium is added, since screening of the ionized electron from the $[Co(\eta\text{-Cp})_2]^+$ attractive potential becomes more effective. This would probably lead to a greater value in $N(E_F)$ for the pure diselenide relative to the disulfide, which would be expected to lead to a decrease in the T_c value as predicted by BCS theory.

3.5 Photoelectron Spectroscopy Experiments

Ultraviolet and *X*-ray photoelectron experiments were carried out on the host and intercalates in order to investigate the perturbations to the band structure and redox states of the host upon intercalation of cobaltocene. In order to carry out surface studies it is essential to have reproducibly clean surfaces. The preparation of clean, undisturbed crystal surfaces was achieved by cleavage of single crystals of both the host lattices and the intercalate samples in ultra-high vacuum (UHV) within the PES spectrometer. The resulting UV and *X*-ray photoelectron spectra of these materials were considered to be of high quality.

In the *X*-ray photoelectron spectra of the hosts and intercalates the main emission peaks due to Sn, S, and Se all remain essentially unchanged upon intercalation retaining similar binding energies accompanied by a small increase in peak widths. However, for Sn(4*d*) emission a weak shoulder appears at lower binding energy to the main peak for all members of the series. By fitting Gaussian lineshapes to the Sn(4*d*) peak it was possible to calculate that the additional species has roughly 10% of the intensity of the main peak for the disulfide case, rising gradually through the series to roughly 12% of the main peak intensity for the diselenide case.

The data are consistent with the formation of a reduced tin species as a result of electron transfer from the nineteen valence electron $Co(\eta\text{-Cp})_2$ guest molecule. The binding energy sepa-

ration of the two species (ΔE_B = 1 eV) is constant as the selenium content changes. Similar binding energy shifts have been obtained for the intercalation of Cu into SnS_2[24] and Ag into $SnSe_2$.[25] It might be expected that a two-electron reduction of the tin site is occurring leading to the formation of a Sn^{II} species. Consequently, two cobaltocene molecules are required to effect the complete reduction of a Sn^{IV} site.

We have also investigated the cobalt emission peaks in the XPS spectra of the intercalate series. In all cases there appears to be at least two resolvable $Co(^2P_{3/2})$ emission peaks at *ca.* 780 and 782 eV. The ratio of these two peaks varies between 1:1.3 and 1:3.1 across the series. The binding energy separation (ΔE_B = 1.8 eV) suggests that the two cobalt species are Co^{2+} and Co^{3+}. These two emission peaks have been assigned to $Co(\eta\text{-Cp})_2$ and $[Co(\eta\text{-Cp})_2]^+$ by comparison with the $Co(^2P_{3/2})$ emission peaks from authentic samples of both $Co(\eta\text{-Cp})_2$ and $[Co(\eta\text{-Cp})_2]^+[PF_6]$. Such results were some of the first to suggest that these classical redox intercalation reactions may not always proceed to complete electron-transfer from the guest to the host and that complex mixed valency species may be formed in the layers. Recent EPR studies on $Cd_2P_2S_6\{Co(\eta\text{-Cp})_2\}_{0.8}$ have also demonstrated the equilibrium of these neutral and ionized cobaltocenes between the layers of $Cd_2P_2S_6$.[26]

The ultraviolet photoelectron (UPS) spectra of the host crystals show the valence band maximum shifting to lower binding energy as the selenium content increases, consistent with the decreasing band gap of the host. In each case there is a dramatic change in the UPS spectra upon intercalation. The spectra can be broadly interpreted as the summation of two subspectra due to the UPS spectra of host lattice and the cobaltocene guests. The additional intensity in the band gap (lowest ionization band) stems from the transfer of electrons to the tin band.

3.6 Impurity Band Model for the Electronic Structure

A qualitative band model description would be useful in understanding the process of electron transfer between the guest and the host. A Rigid Band Model approach would view the intercalate band structure as the sum of the guest and host valence bands (VB) together with the creation of a partially-filled conduction band (CB) by electron transfer. However, the observed changes near the Fermi level suggest that the process of electron transfer does not simply fill the empty Sn(5*s*,5*p*) states in the conduction band to give a metallic system in all cases. The evidence indicates that there are strong electron localizing effects at play, especially in the sulfur-rich intercalates (x = 0.0, 0.3, 0.5), such that simple band theory is inapplicable.

The impurity band model for heavily-doped semiconductors (*e.g.* P/Si) offers a useful approach to the understanding of the intercalate electronic structure. The overlap of the impurity orbitals is significant at high impurity concentrations resulting in the formation of an impurity band close to the conduction band of the semiconductor, as in Figure 7. However, metallic conductivity does not follow directly, since the localizing effects of the impurity potential may be significant. The Hubbard criterion states that the width of the impurity band (W) must be greater than the electron repulsion (U), in order that a delocalized metallic system can form. Indeed, at a critical impurity concentration, the doped system may become metallic.

The substitutional nature of the doping in P/Si is clearly distinct from the reaction that intercalates $Co(\eta\text{-Cp})_2$ into SnX_2 {X = S, Se} hosts, but the guest species can be considered to be an impurity sitting adjacent to the acceptor tin sites. The electron transfer is viewed as an overlap of empty Sn(5*s*,5*p*) states with the filled $Co(\eta\text{-Cp})_2$ dπ* impurity states leading to the formation of an impurity band near the host conduction band. The transfer of an electron onto a Sn^{IV} site creates a strong electron–phonon interaction, such that a second transferred electron gives a Sn^{II} valency; Sn^{III} is commonly observed to disproportionate. The Sn $5s^2$ states that constitute the impurity band form below the main empty conduction band states. The parent $[Co(\eta\text{-Cp})_2]^+$ attractive potential adjacent to the reduced tin site tends to localize the electrons as well. Thus, these mixed valency materials may be pictured as having electrons hopping between the tin and cobaltocene sites. XPS is able to detect two tin oxidation states, the hopping being slow on a XPS timescale.

For $SnS_2\{Co(\eta\text{-Cp})_2\}_{0.33}$ the effects of the lattice distortion at the tin site and the $[Co(\eta\text{-Cp})_2]^+$ impurity potential may be sufficient to localize the transferred electrons into an impurity band in the band gap. Conductivity studies have confirmed the semiconducting character of the disulfide intercalate.

The impurity band width (W) depends on the impurity concentration (n_d) and the width of the host conduction band. The electron repulsion energy (U) depends on the size of the impurity orbitals (Sn $5s^2$), which is directly related to the polarizability of the medium, *i.e.* the screening of the ionized electrons from $[Co(\eta\text{-Cp})_2]^+$ by the medium. Treating the impurity orbitals as hydrogenic with radius a_H, Mott deduced that the transition to the metallic state, as the electron repulsion effects within the impurity band are overcome, is achieved at $n_d^{1/3}a_H$ *ca.* 0.25.[27]

As the sulfur is replaced by selenium in the intercalates the band width of the host conduction band increases and the polarizability of the medium increases, but the impurity con-

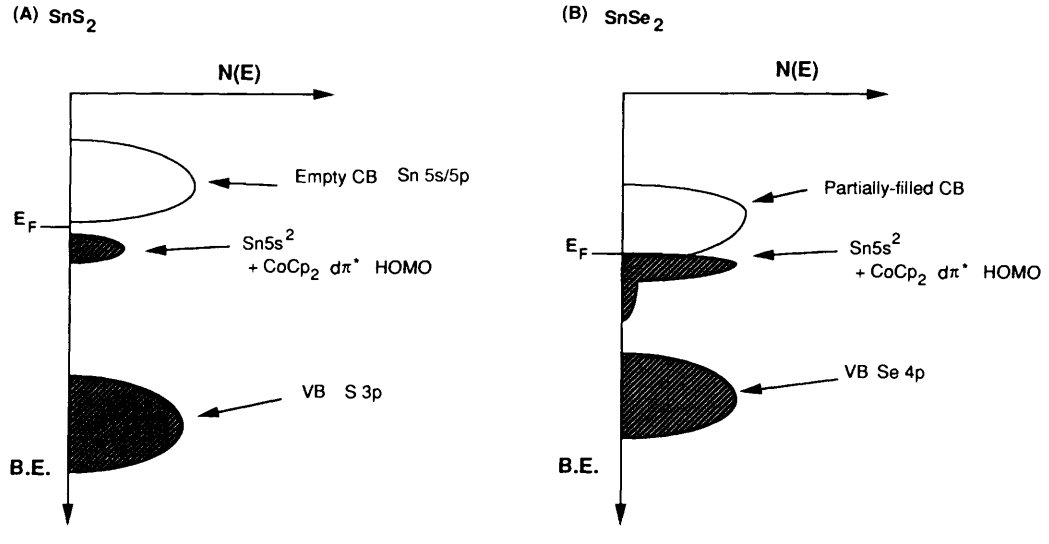

Figure 7 Schematic band structure diagrams for $SnS_2\{Co(\eta\text{-Cp})_2\}_{0.31}$ and $SnSe_2\{Co(\eta\text{-Cp})_2\}_{0.33}$.

centration remains constant (Sn:Co *ca.* 3:1). Thus, the extent of Sn(5*s*,5*p*) and Co(η-Cp)$_2$ dπ* overlap increases to give a shift of the impurity band, eventually giving an extended overlap with the host conduction band such that a transition to metallic behaviour at a critical selenium content ($1.3 < x < 1.85$) occurs. The electrons on the reduced tin sites may now be to some extent itinerant in the impurity band. As we have seen this is consistent with our conductivity measurements on $SnSe_2\{Co(\eta\text{-}Cp)_2\}_{0.33}$ which confirm the metallic character of this material and reveal that it is a type II superconductor.

4 Conclusions

The intercalation of cobaltocene into single crystals of the layered tin dichalcogenides $SnS_{2-x}Se_x$ presented us with a unique opportunity to study in detail the structural and electronic changes taking place on intercalation of this highly electron-rich organometallic compound. The *X*-ray and neutron diffraction analyses clearly show that the molecules adopt a highly ordered arrangement within the layers and surprisingly with the principal axis of the cobaltocene parallel to the basal planes of the lattice. The most remarkable observation is the dramatic change in the electrical conductivity across the series. The totally unexpected observation of superconductivity for $SnS_{2-x}Se_x\{Co(\eta\text{-}Cp)_2\}_{0.33}$ $\{1.85 \leqslant x \leqslant 2\}$ has given impetus to further work and demonstrated that there are still fascinating discoveries to be made in this area of chemistry.

Acknowledgments. The author is grateful to acknowledge support from the Science and Engineering Research Council and the Nuffield Foundation. I also thank my co-workers (C. A. Formstone, E. T. FitzGerald, P. A. Cox, M. Kurmoo, K. Prout, H.-V. Wong, C. Grey, J. Hodby, J. S. O. Evans, and S. J. Heyes) for their contributions to the work reported herein.

5 References

1 R. H. Friend and A. D. Yoffe, *Adv. Phys.*, 1987, **36**, 1; 'Physics and Chemistry of Materials with Layered Structure', Vol. 4, ed. P. A. Lee, Reidel, Dordrecht, 1976.
2 H. P. B. Rimmington and A. A. Balchin, *Phys. Status Solidi*, 1971, **6**, K47.
3 'Intercalation Chemistry', ed. M. S. Whittingham and A. J. Jacobson, Academic Press, New York, 1982.
4 F. R. Gamble, F. J. DiSalvo, R. A. Klemm, and T. H. Geballe, *Science*, 1970, 568.
5 D. C. Johnston, *Solid State Commun.*, 1982, **43**, 533.
6 P. C. Klipstein and R. H. Friend, *J. Phys. C.*, 1984, **17**, 2713.
7 F. S. Ohuchi, W. Jaegermann, C. Pettenkofer, and B. A. Parkinson, *Langmuir*, 1989, **5**, 439.
8 R. B. Somoano and A. Rembaum, *Phys. Rev. Lett.*, 1971, **27**, 402.
9 B. Bach and J. M. Thomas, *J. Chem. Soc., Chem. Commun.*, 1972, 301.
10 M. S. Whittingham, *Prog. Solid State Chem.*, 1978, **12**, 41.
11 L. Benes, J. Votinsky, P. Lostak, J. Kalousova, J. Klikorka, *Phys. Status Solidi*, 1985, **89**, K1; J. Votinsky, L. Benes, J. Kalousova, P. Lostak, and J. Klikorka, *Chem. Papers*, 1988, **42**, 133.
12 D. O'Hare, J. S. O. Evans, P. J. Wiseman, and K. Prout, *Angew. Chem., Int. Ed. Engl.*, 1991, **30**, 1156.
13 C. A. Formstone, E. T. FitzGerald, P. A. Cox, and D. O'Hare, *Inorg Chem.*, 1990, **29**, 3860.
14 C. A. Formstone, E. T. FitzGerald, P. A. Cox, D. O'Hare, and M. J. Kurmoo, *J. Mater. Chem.*, 1991, **1**, 51.
15 C. Grey, J. S. O. Evans, D. O'Hare, and S. J. Heyes, *J. Chem. Soc., Chem. Commun.*, 1991, 1380.
16 M. B. Dines, *Science*, 1975, **188**, 1210.
17 R. P. Clement, W. B. Davies, K. A. Ford, M. L. H. Green, and A. J. Jacobson, *Inorg. Chem.*, 1978, **17**, 2754.
18 J. S. Miller and A. J. Epstein, *Angew. Chem., Int. Ed. Engl.*, 1987, **63**, 287.
19 N. F. Mott and E. A. Davies, 'Electronic Processes in Non-Crystalline Materials', Clarendon, Oxford, 2nd Edn. 1979; M. A. Kastner, R. J. Birgeneau, C. Y. Chen, Y. M. Chiang, D. R. Gabbe, H. P. Jenssen, T. Yunk, C. J. Peters, P. J. Picone, T. Thio, T. R. Thurston, and H. L. Tuller, *Phys. Rev. B*, 1988, **37**, 111.
20 B. Fotouhi, A. Katty, and R. Parsons, *J. Electroanal. Chem.*, 1985, **183**, 303.
21 Y. Frongillo, M. Aubin, and S. Jandl, *Can. J. Phys.*, 1985, **63**, 1405.
22 N. F. Mott and E. A. Davies, 'Electronic Processes in Non-Crystalline Materials', Clarendon, Oxford, 2nd Edn., 1979.
23 V. Ambegaokar, B. I. Halperin, and J. S. Langer, *Phys. Rev. B*, 1971, **4**, 2612.
24 F. S. Ohuchi, W. Jaegermann, and B. A. Parkinson, *Surf. Sci.*, 1988, **194**, L69.
25 C. Formstone and P. A. Cox, Unpublished work.
26 D. A. Cleary and A. H. Francis, *J. Phys. Chem.*, 1985, **89**, 97.
27 P. P. Edwards and M. J. Sienko, *J. Am. Chem. Soc.*, 1981, **103**, 2967.